Structure: Function Studies of the Cytosolic, Mo- and NAD⁺-Dependent Formate Dehydrogenase from *Cupriavidus necator*

Russ Hille [1,*], Tynan Young [2], Dimitri Niks [1], Sheron Hakopian [3], Timothy K. Tam [2], Xuejun Yu [4], Ashok Mulchandani [5] and Gregor M. Blaha [1,*]

[1] Department of Biochemistry, University of California, Riverside, CA 92521, USA; dimitri.niks@ucr.edu
[2] Department of Biochemistry and the Biochemistry and Molecular Biology Graduate Program, University of California, Riverside, CA 92521, USA; tynan.young@email.ucr.edu (T.Y.); ttam004@ucr.edu (T.K.T.)
[3] Department of Biochemistry and the Environmental Toxicology Graduate Program, University of California, Riverside, CA 92521, USA; shako001@ucr.edu
[4] Bioengineering Graduate Program, University of California, Riverside, CA 92521, USA; xyu010@ucr.edu
[5] Department of Chemical and Environmental Engineering, University of California, Riverside, CA 92521, USA; adani@engr.ucr.edu
*   Correspondence: russ.hille@ucr.edu (R.H.); gregor.blaha@ucr.edu (G.M.B.); Tel.: +1-951-827-6354 (R.H.); +1-951-827-4294 (G.M.B.)

Abstract: Here, we report recent progress our laboratories have made in understanding the maturation and reaction mechanism of the cytosolic and NAD⁺-dependent formate dehydrogenase from *Cupriavidus necator.* Our recent work has established that the enzyme is fully capable of catalyzing the reverse of the physiological reaction, namely, the reduction of CO_2 to formate using NADH as a source of reducing equivalents. The steady-state kinetic parameters in the forward and reverse directions are consistent with the expected Haldane relationship. The addition of an NADH-regenerating system consisting of glucose and glucose dehydrogenase increases the yield of formate approximately 10-fold. This work points to possible ways of optimizing the reverse of the enzyme's physiological reaction with commercial potential as an effective means of CO_2 remediation. New insight into the maturation of the enzyme comes from the recently reported structure of the FdhD sulfurase. In *E. coli*, FdhD transfers a catalytically essential sulfur to the maturing molybdenum cofactor prior to insertion into the apoenzyme of formate dehydrogenase FdhF, which has high sequence similarity to the molybdenum-containing domain of the *C. necator* FdsA. The FdhD structure suggests that the molybdenum cofactor may first be transferred from the sulfurase to the C-terminal cap domain of apo formate dehydrogenase, rather than being transferred directly to the body of the apoenzyme. Closing of the cap domain over the body of the enzymes delivers the Mo-cofactor into the active site, completing the maturation of formate dehydrogenase. The structural and kinetic characterization of the NADH reduction of the FdsBG subcomplex of the enzyme provides further insights in reversing of the formate dehydrogenase reaction. Most notably, we observe the transient formation of a neutral semiquinone FMNH·, a species that has not been observed previously with holoenzyme. After initial reduction of the FMN of FdsB by NADH to the hydroquinone (with a k_{red} of 680 s⁻¹ and K_d of 190 μM), one electron is rapidly transferred to the Fe_2S_2 cluster of FdsG, leaving FMNH·. The Fe_4S_4 cluster of FdsB does not become reduced in the process. These results provide insight into the function not only of the *C. necator* formate dehydrogenase but also of other members of the NADH dehydrogenase superfamily of enzymes to which it belongs.

Keywords: nicotinamide adenine dinucleotide (NADH); electron transfer; enzyme kinetics; enzyme structure; formate dehydrogenase; carbon assimilation

1. Introduction

The molybdenum- and tungsten-dependent formate dehydrogenases have drawn increased attention over the past 5–10 years due to the demonstration that under the appropriate conditions, most, if not all, are able to catalyze the reverse reaction, reduction of CO_2 to formate, under the appropriate conditions. Indeed, some enzymes of this family, which include the closely related formylmethanofuran dehydrogenases of the Wood–Ljungdahl pathway, function physiologically to reduce CO_2 to formate in what is probably the most evolutionarily ancient mechanism of carbon fixation.

Cupriavidus necator H16 (previously known as *Ralstonia eutropha*) has four formate dehydrogenases, of which, two are cytosolic enzymes that utilize NAD^+ as oxidizing substrate [1,2]. One of these contains molybdenum and is encoded by the *fdsGBACD* operon, the other possesses tungsten and is encoded by the *fdwAB* operon (presumably enlisting additional subunits from the *fds* operon) [3]. The molybdenum-containing enzyme was originally isolated and characterized by Bowien and coworkers, who showed that the mature holoenzyme belongs to the NADH dehydrogenase superfamily of enzymes [4–6]. The FdsA, FdsB, and FdsG subunits are homologous to corresponding subunits in the cytosolic arm of NADH dehydrogenase [7–10]. FdsA is homologous to the Nqo3 subunit of the NADH dehydrogenase from *Thermus thermophilus* [8,9], although the latter lacks a molybdenum center as found in the former [7]. The homology between FdsA and Nqo3 includes the presence of a histidine ligand to one of the Fe_4S_4 clusters. The C-terminal domain of FdsA, containing the molybdenum center, is also homologous to the crystallographically characterized FdhF formate dehydrogenase of *E. coli*, with the molybdenum-coordinating Cys 378 of FdsA equivalent to Sec 140 in FdhF [11]. The Fe_4S_4- and FMN-containing FdsB subunit is homologous to the *T. thermophilus* Nqo1 subunit and like Nqo1 also possesses a binding site for $NADH/NAD^+$. The FdsG subunit is homologous to the *T. thermophilus* Nqo2 subunit and has a single Fe_2S_2 cluster. We report here recent work from our laboratories on both mechanistic and structural aspects of the *C. necator* enzyme.

2. Catalysis of CO_2 Reduction by the *C. necator* Formate Dehydrogenase

Under physiological conditions, reducing equivalents enter the *C. necator* formate dehydrogenase holoenzyme at its molybdenum center and leave at the FMN, reducing NAD^+ to NADH; electron transfer between the molybdenum and flavin, which are separated by some 55 Å [10], is mediated by the intervening iron–sulfur clusters. Although originally reported to be unable to catalyze the CO_2 by NADH, we have recently shown that the enzyme is indeed capable of doing so when CO_2 (not bicarbonate) is used as substrate [12]. This is consistent with a mechanism for formate oxidation involving direct hydride transfer of the C_α-H to the $Mo^{VI} = S$ group of the $L_2Mo^{VI}S(S-Cys)$ molybdenum center (where L is the bidentate enedithiolate-coordinated pyranopterin cofactor found in molybdenum- and tungsten-containing enzymes, present in this enzyme as the guanine dinucleotide) to $L_2Mo^{IV}(SH)(S-Cys)$, with CO_2 rather than bicarbonate as the immediate product of the reaction [13]. The steady-state kinetic parameters have been determined in both the forward and reverse directions and are shown in Table 1.

**Table 1.** Steady-state kinetic parameters for the *C. necator* formate dehydrogenase.

	Forward	**Reverse**
k_{cat}	201 s^{-1}	10 s^{-1}
$K_m^{formate}$	130 μM	–
K_m^{NAD+}	310 μM	–
K_m^{CO2}	–	2700 μM
K_m^{NADH}	–	46 μM

The Haldane relationship for these parameters for an enzyme, such as formate dehydrogenase operating via a ping-pong mechanism with separate sites for the reductive and oxidative half-reactions, is as follows:

$$K_{eq} = \frac{\left(k_{cat}^{forward}\right) \cdot \left(k_{cat}^{forward}\right)}{\left(K_m^{formate}\right) \cdot \left(K_m^{NAD+}\right)} = \frac{\left(201 \text{ s}^{-1}\right) \cdot \left(201 \text{ s}^{-1}\right)}{\left(130 \text{ μM}\right) \cdot \left(310 \text{ μM}\right)} = 1250 \tag{1}$$
$$\frac{\left(k_{cat}^{reverse}\right) \cdot \left(k_{cat}^{reverse}\right)}{\left(K_m^{CO_2}\right) \cdot \left(K_m^{NADH}\right)} \quad \frac{\left(10 \text{ s}^{-1}\right) \cdot \left(10 \text{ s}^{-1}\right)}{\left(2700 \text{ μM}\right) \cdot \left(46 \text{ μM}\right)}$$

The value 1250 compares favorably with the K_{eq} calculated from the 100 mV difference between $\Delta E_{0'}$ for the NAD^+/NADH and CO_2/formate couples of 2100, the disparity reflecting a ~10% uncertainty in $k_{cat}^{forward}$ and $k_{cat}^{reverse}$, which are squared terms in numerator and denominator, respectively, of Equation (1).

The reaction can be pushed significantly in the direction of CO_2 reduction by the addition of an NADH regeneration system [14]. As shown in Figure 1 left, addition of a catalytic amount of formate dehydrogenase to a solution that is 29.5 mM in CO_2 (at 30 °C) and 300 μM in NADH results in the formation of 120 μM formate (as quantified by ion chromatography) and 130 μM NAD^+—in other words, the reaction is tightly coupled. When the experiment is repeated with the addition of 50 mM glucose and a catalytic amount of glucose dehydrogenase for NADH regeneration, the amount of formate generated increases approximately 10-fold to 1.0 mM (Figure 1 right). This illustrates the potential commercial use of the enzyme for generation of formate from CO_2 using a suitable source of reducing equivalents.
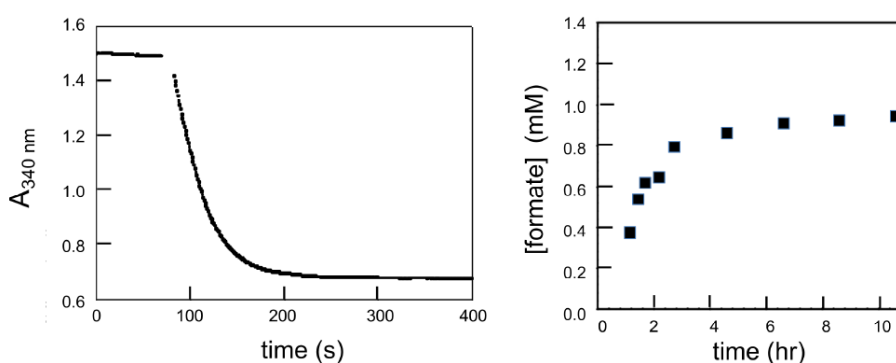

Figure 1. Catalysis of CO_2 reduction to formate by *C. necator* formate dehydrogenase. (**Left**) the reaction of 0.2 μM holoenzyme with 29.5 mM CO_2 (aq) and 300 μM NADH, 20 mM Bis-Tris propane, pH 6.3, 30 °C. The absorbance change reflects the consumption of 130 μM NADH. The amount of formate accumulated as determined by ion chromatography was 120 μM [12]. (**Right**) the accumulation of formate under the same conditions upon addition of 50 mM glucose and catalytic glucose dehydrogenase to the reaction mix. Adapted with permission from *Biochemistry* **2019**, *58*, 1861–1868 [14]. Copyright (2019) American Chemical Society.

3. Insertion of the Molybdenum Cofactor into Formate Dehydrogenase and Other Members of the DMSO Reductase Family

As is seen with all members of the DMSO reductase family of molybdenum enzymes, the active site molybdenum center is deeply buried in the C-terminal domain of the FdsA subunit, and the means by which it is introduced into the apoenzyme is not presently understood. Given the extensive structural homology of this domain to the *E. coli* FdhF, one can consider the overall topology of the latter which consists of three interlaced domains that constitute the body of the protein, and a contiguous C-terminal domain that constitutes a "cap" over the cofactor in the holoenzyme (Figure 2A [11]). It is now well-accepted that all the Mo- and W-containing formate dehydrogenases possess a M=S group that is inserted into the metal coordination sphere as the final step of cofactor maturation [15]. Sulfur forms a more covalent bond with molybdenum and tungsten than does the more electronegative oxygen. As a result, there is less formal negative charge on the sulfur, e.g., making it better able to accept a hydride in

the course of the reaction. A similar argument has been made in the case of xanthine oxidase and related enzymes, which also require a Mo=S [10]. The sulfur transferase catalyzing this reaction (the product of the *fdhD* gene in *E. coli*, *fdsC* in the *C. necator* operon) is also thought to play a role in the insertion process, and the X-ray crystal structure of FdhD has recently been reported with two equivalents of GDP bound at the presumed position of the maturing molybdenum center [16]. Modeling the cofactor into the structure yields a complex with the apex of the molybdenum coordination sphere pointing into the channel through which the catalytically essential sulfur is delivered (via a cysteine desulfurase), with the *bis*(MGD) portion of the cofactor presenting a concave basket to the surface of the complex; the pyranopterin portion of both cofactors is solvent-exposed with the principal interactions with FdhD principally involving the guanine dinucleotide extensions of the cofactor (Figure 2B). In this orientation, the cofactor cannot be transferred directly to the body of the apo FdhF, where it is also oriented concave outwards with the two guanine dinucleotide arms extended into the protein, not out toward solvent. On the other hand, the molybdenum center in FdhF interacts with the cap domain of the protein principally via its pyranopterin rings, interacting minimally with the guanine dinucleotide arms. This being the case, it is possible to dock the cap (with bound cofactor) to the dimeric FdhD$_2$·(GDP)$_2$ complex in such a way that the GDP arms overlap; both proteins are in a position to interact optimally with the cofactor sandwiched between them. If this interaction is physiologically significant, the implication is that FdhD passes the now sulfurated and mature cofactor not to the body of apo FdhF but to its cap, which then closes over the body swinging the cofactor into position in the active site. In this way the highly unstable cofactor is never released into free solution. There have been a number of efforts in the past to identify regions on the surface of DMSO reductase family enzymes that interact with the cofactor insertion machinery. If the above analysis is correct, then this surface, on the face of the C-terminal cap domain that interfaces with the body of the enzyme, is buried in the structure of the holoenzyme. In support of this model, the C-terminal cap domains of the apo forms of both *E. coli* trimethylamine-*N*-oxide reductase TorA [17] and *E. coli* periplasmic nitrate reductase NapA [18] in complex with their respective chaperones TorD and NapD (that recognize the proteins' N-terminal twin-Arg signal sequence that targets them to the periplasm) have been reported to assume an open position in readiness to accept the mature molybdenum cofactor. This indicates that the C-terminal cap domain is indeed able to adopt the type of open configuration that is proposed here.
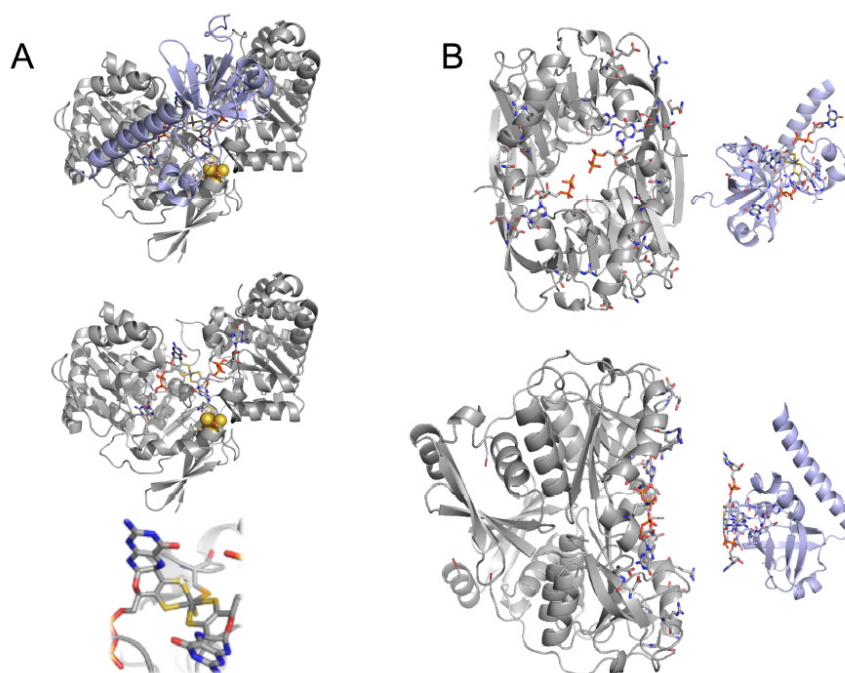
Figure 2. A comparison of the structures of FdhD and FdhF. Panel (**A**) top, the structure of FdhF (PDB 1FDO), with the body of the enzyme in *gray* and the C-terminal cap domain in *blue*. Middle, the body

of FdhF with the C-terminal cap domain removed, revealing the buried molybdenum center. Bottom, an enlargement of the molybdenum center, illustrating its disposition in the body of FdhF. Panel (**B**) top, views of the putative interfaces of the dimeric FdhD in complex with two equivalents of GDP (*gray*; PDB 4PDE) and the C-terminal cap domain of FdhF with the molybdenum center shown (*blue*). Bottom, the structures shown rotated toward one another illustrating the overlap between the GDP's of the FdhD structure and the molybdenum center of FdhF.

4. The Crystal Structure of FdsBG

The X-ray crystal structure of the FdsBG subcomplex of the *C. necator* formate dehydrogenase has also been determined at a resolution of 2.3 Å [19]. This fragment of the holoenzyme contains FMN and a Fe_4S_4 cluster in the FdsB subunit and a Fe_2S_2 cluster in FdsG; it lacks the FdsA subunit that contains the molybdenum center and additional iron–sulfur clusters. As expected, the structure of each subunit is closely related to its cognate subunits in the NADH dehydrogenases from *T. thermophilus* and *Aquifex aeolicus*, FdsB being homologous to the *T. thermophilus* Nqo2 and *A. aeolicus* NuoF subunits and contains FMN and a Fe_4S_4 cluster, and FdsG to the *T. thermophilus* Nqo1 and *A. aeolicus* NuoE subunits and contains a Fe_2S_2 cluster [20]. Compared to the *A. aeolicus* NuoF, FdsB has an RMSD of 1.48 Å for 394 C_α atoms and contains a Rossmann-like fold [21] encompassing the FMN binding site, a ubiquitin-like and a four-helix domain containing the Fe_4S_4 cluster [22] (Figure 3); all these structural elements are shared with NuoF. The Fe_4S_4 cluster is in a mostly hydrophobic environment close to the protein surface and is bound by C443[B], C446[B], C449[B], and C489[B] (superscript B indicating the residue is in FdsB). The principal structural differences between FdsB and NuoF are in surface loops of the protein. However, the N-terminal portion of FdsB consists of a thioredoxin-like fold [20] not seen in NuoF or Nqo1. This domain lacks the Fe_2S_2 cluster typical of thioredoxins owing to mutation of the iron-coordinating cysteines (P10[B], A15[B], S45[B], and F49[B]). This resembles the C-terminal portion of FdsG (RMSD 1.97 Å for 71 $C\alpha$ atoms of the core of the domain) that contains the Fe_2S_2 cluster (vide infra).

The FdsG subunit is homologous to the NuoE subunit of *A. aeolicus* NADH dehydrogenase, consisting of an N-terminal four-helical bundle (residues 29[G]–74[G]) and a C-terminal thioredoxin-like domain (residues 79[G]–159[G]) that possesses the subunit's Fe_2S_2 cluster. These two domains are connected by a four-amino acid linker and are rotated by ~26° relative to the orientation seen in NuoE.

It is to be noted that while the N-terminal domains of FdsG and NuoE both have four helices, the first helix of FdsG runs parallel, but in NuoE, it runs across the second and third helices. The C-terminal thioredoxin-like domain of FdsG resembles the N-terminal thioredoxin-like domain of FdsB, but unlike the cofactorless FdsB domain, the FdsG domain contains a spinach ferredoxin-like Fe_2S_2 cluster [19]. This iron–sulfur cluster is again in a hydrophobic environment near the surface, coordinated by C86[G], C91[G], C127[G], and C131[G]. Like *A. aeolicus* NuoE (but unlike *T. thermophilus* Nqo1), the C-terminus of FdsG is truncated at its C-terminus and lacks a disulfide bond.

At the FdsB–FdsG interface, two helices of the N-terminal four-helical bundle domain of FdsG contact the Rossmann-like domain of FdsB, as seen in the subunit interface between NuoE and NuoF. FdsG's C-terminal thioredoxin-like domain interacts with the same surfaces of the ubiquitin-like and Rossmann-like domains of FdsB as do the corresponding structural elements of NuoE and NuoF. The different placement of the ubiquitin and of the 183[B]–190[B] loop in FdsB as compared to NuoE results in an increase in the distance between the Fe_2S_2 cluster of FdsG and the Fe_4S_4 cluster of FdsB, being of ~1.0 Å as compared to the separation seen in NuoEF.

At a distance of nearly 21 Å (edge-to-edge), direct electron transfer between the two Fe/S clusters is expected to be extremely slow and unlikely to be physiologically relevant. On the other hand, each cluster is within 12 Å of the FMN isoalloxazine ring (Figure 4). Given the model that has been constructed for the holoenzyme based on the structures of FdhF and Nqo123, the Fe_4S_4 cluster of FdsB clearly lies on-path for electron transfer between the molybdenum center and FMN of the formate dehydrogenase, while the Fe_2S_2 cluster of FdsG is off-path. In the NADH dehydrogenases, it has been

suggested that this cluster may serve to temporarily store electrons during electron transfer out of the FMN once it has been reduced by NADH (vide infra). The FMN in FdsB is surrounded by a network of interactions that is also conserved in other NADH dehydrogenase-like enzymes [20,23] and is part of the solvent-accessible cavity that constitutes the NAD^+/NADH binding site. The C8-methyl of the FMN points towards the Fe_4S_4 cluster, with the C_4=O facing the Fe_2S_2 cluster (Figure 4).
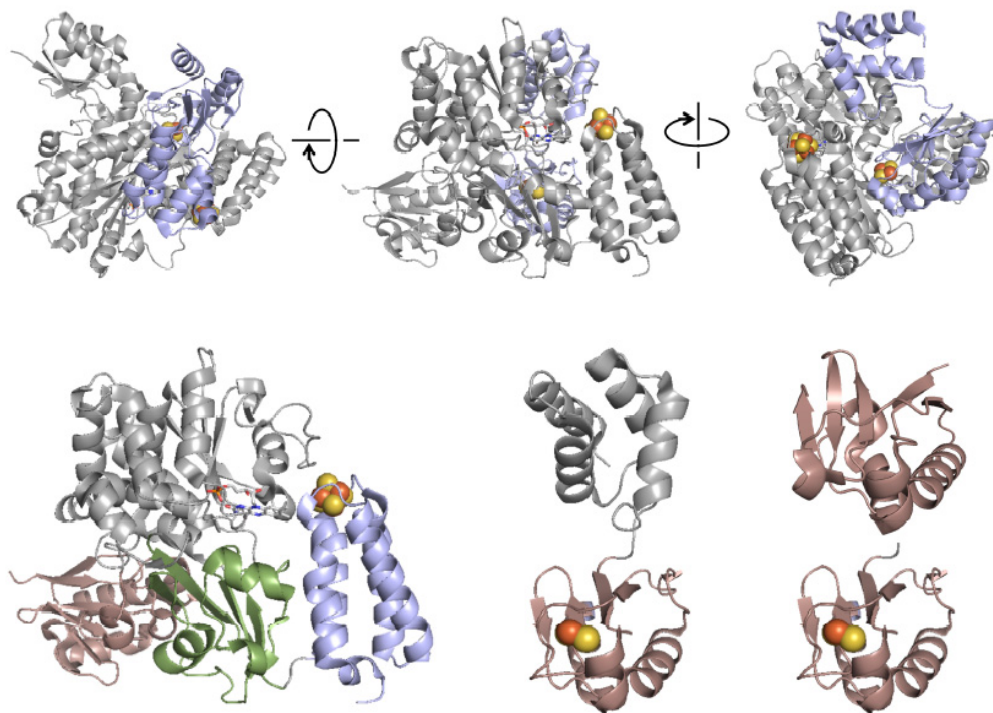
Figure 3. The structure of FdsBG. (**Top**) the overall structure of FdsBG, with FdsB in *gray* and FdsG in *blue* (PDB 6VW8). The center structure is rotated about the horizontal or vertical axis as indicated to give the structures to the left and right, respectively. The two iron–sulfur clusters are rendered as CPK spheres and the FMN as CPK sticks. (**Bottom Left**) the domain structure of FdsB, with the thioredoxin-like domain in *red*, the Rossmann fold in *gray*, the ubiquitin-like domain in *green*, and the four-helix domain in *blue*; (**Center**) the domain structure of FdsG, with the N-terminal domain in gray and the thioredoxin-like domain in *red*; (**Right**) a comparison of the thioredoxin-like domains of FdsB (*upper*) and FdsG (*lower*).
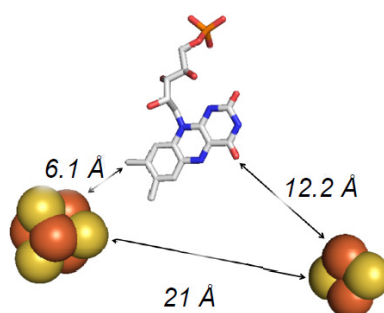

Figure 4. Disposition of the redox-active centers of FdsBG. From left to right the Fe_4S_4 and FMN of FdsB and the Fe_2S_2 of FdsG (PDB 6VW8).

5. EPR Characterization of the Iron–Sulfur Clusters of FdsBG

Extended incubation of FdsBG complex with sodium dithionite (pH 7.0) yields two signals (as seen in Figure 5 top). The first is seen at liquid nitrogen temperatures as high as 200 K, with $g_{1,2,3}$ = 2.000, 1.948, and 1.920 and linewidths of 1.4, 1.7, and 1.6 mT, respectively. These values are in good agreement

with previously reported parameters for the cluster designated as Fe/S$_1$ for holoenzyme (Figure 5 middle, dotted spectrum) [13]. The second signal is seen only below 20 K and has g$_{1,2,3}$ = 2.039, 1.955, and 1.891, and linewidths of 4.5, 1.4, and 5.3 mT (Figure 5 middle, dashed spectrum). This signal has not been previously seen with the holoenzyme [13], owing to its low intensity, broad linewidths, and overlap with the much stronger Fe/S$_3$ signal, and is designated Fe/S$_5$. In the *A. aeolicus* NuoEF and *T. thermophilus* Nqo12 NADH dehydrogenases, only the Fe$_2$S$_2$ clusters exhibit EPR signals at 77 K, while the Fe$_4$S$_4$ signals appear only below 50 K [24]. Further, the g-values g$_{1,2,3}$ = 2.004, 1.945, and 1.917 for the N1a Fe$_2$S$_2$ cluster of the 24 kDa subunit of bovine complex I [25] (the homolog to FdsG) are in very good agreement with the Fe/S$_1$ signal seen here in FdsBG, and accordingly, the Fe/S$_1$ signal has been assigned to the Fe$_2$S$_2$ cluster of FdsG. The signal assigned to the N3 Fe$_4$S$_4$ cluster in the NADH dehydrogenase systems, with g-values of g$_{1,2,3}$ = 2.037, 1.945, and 1.852, is also in good agreement with the Fe/S$_5$ signal of the FdsBG complex, and we accordingly assign the Fe/S$_5$ signal to the Fe$_4$S$_4$ cluster of FdsB. The Fe/S$_1$ signal seen with holoenzyme was initially assigned to the His-coordinated Fe$_4$S$_4$ cluster of FdsA (Figure 5 bottom, dotted spectrum) [13], but that is clearly incorrect as FdsBG exhibits the signal. The Fe/S$_5$ signal has similar g-values to those reported for the previously observed Fe/S$_3$, but the signal-giving cluster couples to the molybdenum center and must be the proximal Fe$_4$S$_4$ cluster to the molybdenum center in FdsA; the Fe/S$_5$ signal must, therefore, be a new signal not seen previously with holoenzyme. The assignment of EPR signal Fe/S$_5$ to the Fe$_4$S$_4$ cluster of FdsB is consistent with our previously published structural model of holoformate dehydrogenase placing the Fe$_4$S$_4$ cluster near FdsA in the intact holoenzyme and on-path between the molybdenum and FMN of the enzyme [10].
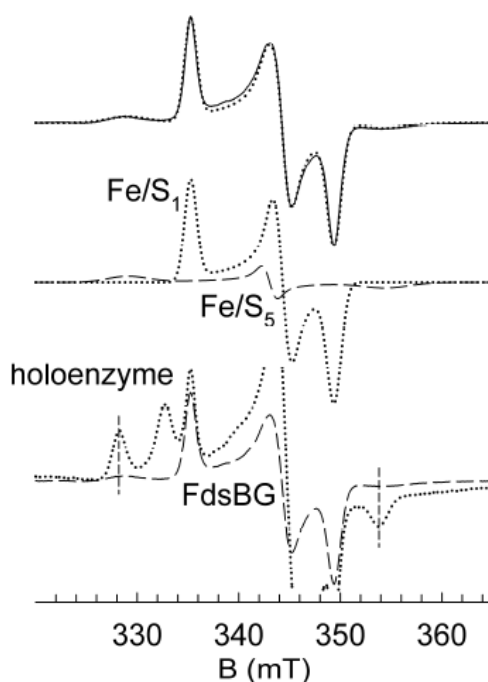
Figure 5. EPR spectra of the iron–sulfur clusters of the FdsBG complex. (**Top**) the observed iron–sulfur EPR spectrum (solid) and simulated composite spectrum (dashed) of dithionite-reduced FdsBG, collected at 9 K with modulation amplitude of 8 Gauss and microwave power of 2 μW. The sample was prepared by incubation of 125 μM of FdsBG complex in 100 mM potassium phosphate, pH 7.0 with 2 mM buffered sodium dithionite under anaerobic conditions for 1 h at room temperature prior to freezing. (**Middle**) the individual signals resulting from the simulation of the composite spectrum above. The spectrum corresponding to the previously assigned Fe/S$_1$ (dotted) and an additional Fe/S$_5$ signal (dashed) are resolved only in the FdsBG complex. (**Bottom**) a comparison of the spectra seen with FdsBG (dashed) and holoenzyme, at 20 K (dotted). The dashed lines mark the location of g$_1$ and g$_3$ features of the Fe/S$_3$ component seen in the spectrum of the reduced holoenzyme (see text) [19].

6. Rapid-Reaction Kinetics of FdsBG Reduction by NADH

The rapid-reaction kinetics of FdsBG reduction by NADH have also been examined. This is the reverse of the physiological reaction for the formate dehydrogenase, but is the physiological direction seen in the NADH dehydrogenases. A typical kinetic transient is shown in the inset of Figure 6 left. The reaction is biphasic, with the fast phase of the reaction completing within 120 ms. A plot of the observed k_{fast} as a function of NADH is hyperbolic (Figure 6 left), yielding a limiting k_{red} of 680 s^{-1} and K_d^{NADH} of 190 μM at 5 °C. We note that this rate is more than sixfold faster than the limiting rate of reduction of holoenzyme at high formate, some 20-fold faster than k_{cat} for formate oxidation (13), and 350-fold faster than k_{cat} for CO_2 reduction [12] under comparable conditions.
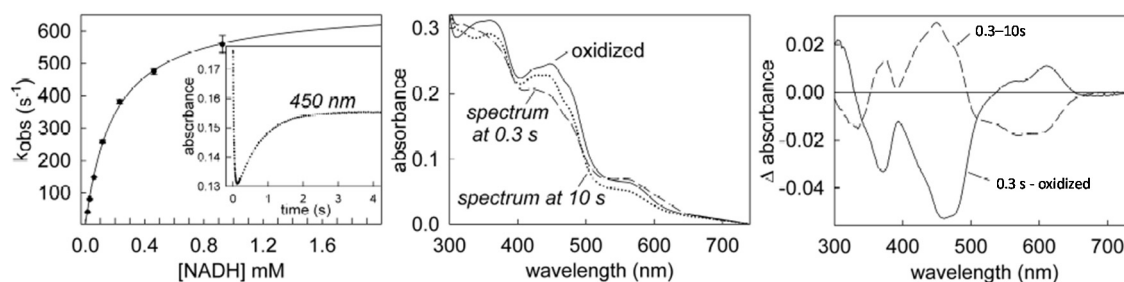
Figure 6. The kinetics of FdsBG reduction by NADH. (**Left**) a plot of k_{fast} vs. NADH, yielding a limiting k_{red} of 680 s^{-1} and a K_d^{NADH} of 190 μM. The *inset* shows a typical biphasic transient, as described in the text. The reaction conditions were 100 mM potassium phosphate, pH 7.0, 5 °C. (**Center**) spectra seen at the times indicated in the reaction of 10 μM FdsBG with 5 μM NADH, as obtained with a photodiode array detector on the stopped-flow. (**Right**) difference spectra obtained using the spectra obtained at the times indicated. The formation of FMNH· in the fast phase of the reaction is reflected in the positive feature in the 500–650 nm region in the *dotted* difference spectrum and its loss during the slow disproportionation phase of the reaction by the negative feature in the same region in the *dashed* difference spectrum [19].

When the reaction was repeated using substoichiometric NADH (so that the FdsBG$_{1e}$- formed on disproportionation will not be further reduced by reaction with a second equivalent of NADH), the absorbance increase seen at the end of the fast phase of the reaction implies formation of the neutral semiquinone FMNH· (Figure 6 center, dashed). This species has not seen in previous work with holoenzyme and must be the result of transfer of a single electron from the fully reduced flavin hydroquinone (formed on its initial two-electron reduction by NADH) to the Fe_2S_2 cluster of FdsG iron, leaving the flavin as FMNH· (and giving rise to the Fe/S$_1$ EPR signal; see further below and Scheme 1). On a second, slower timescale, two equivalents of the FdsBG$_{2e}$- formed upon reaction with NADH disproportionate to give one equivalent each of FdsBG$_{1e}$- and FdsBG$_{3e}$-. To the extent this occurs, FdsBG$_{1e}$- will have its Fe_2S_2 cluster (Fe/S$_1$) reduced and its FMN oxidized, whereas FdsBG$_{3e}$- will have both Fe/S$_1$ and the FMN reduced.
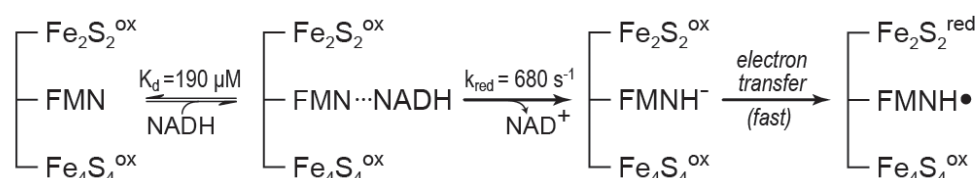

Scheme 1. Proposed electron transfer in FdsBG upon NADH reduction.

The UV/Visible signature of FMNH· [26] is seen as the positive feature in the 500–650 nm region in the difference spectrum between fully oxidized enzyme and that collected at 0.3 s after the initial reaction of FdsBG with NADH (Figure 6 right, black spectrum). The extended negative feature in the 300–500 nm region is due to reduction of the Fe/S clusters. The subsequent disappearance of the

FMNH· formed in the fast phase of the reaction is reflected in the pronounced negative feature in the 500–650 nm region seen in the 0.3–10 s difference spectrum (Figure 6 right, dashed difference spectrum). Here, the two broad, negative peaks centered at 570 and 605 nm reflect the presence of FMNH· at 0.3 s but its loss over the next 10 s. Formation of FMNH· has independently been confirmed in a freeze-quench EPR experiment. Figure 7 shows the spectrum seen at 150 K when FdsBG is reacted with NADH and frozen after ~40 ms (Top), which exhibits the EPR signatures of both FMNH· and Fe/S_1. In addition to demonstrating the formation of FMNH·, this experiment establishes that it is the Fe_2S_2 cluster of FdsG that becomes reduced in forming FMNH·. Subtracting out the Fe/S_1 signal from the measured EPR spectrum yields an isotropic EPR signal with a g_{iso} = 2.003 and a linewidth of ~1.9 mT, reflecting formation of the neutral rather than anionic semiquinone (Figure 7 middle) [27,28]. No additional iron–sulfur signal attributable to the Fe/S_4 signal is seen at 9 K, even when the experiment is repeated in the presence of excess NADH, indicating that it does not get reduced in the course of reduction of FdsBG by NADH (Figure 7 bottom).
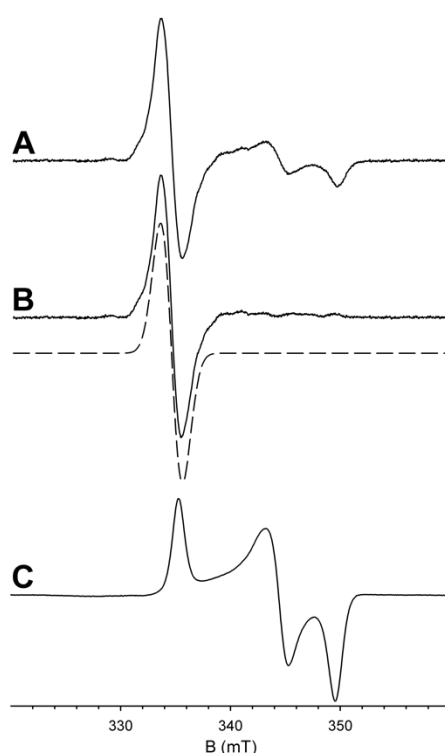
Figure 7. EPR of the neutral flavin semiquinone of FdsBG. (**Top**) The EPR spectrum seen by rapid-freeze quench (quenching time ~40 ms) on reaction of 40 μM FdsBG with 0.8 mM NADH at 0 °C. The spectrum was obtained at 150 K with modulation amplitude of 8 Gauss and microwave power of 0.4 mW. (**Middle**) the spectrum of FADH·, obtained by subtracting out the Fe/S1 contribution (solid line) along with a simulation (dashed line). (**Bottom**) The EPR spectrum seen on mixing 160 μM of FdsBG with 60 μM NADH at room temperature for 10 s prior to freezing. The EPR spectrum was collected at 9 K with modulation amplitude of 8 Gauss and microwave power of 2 μW, and it exhibits only the Fe/S_1 signal with no contribution from Fe/S_4. All samples were prepared in 100 mM potassium phosphate, pH 7.0, under anaerobic conditions [19].

7. The Thioredoxin-Like Domain of FdsB

The N-terminal thioredoxin-like domain of FdsB is extremely similar to the Fe_2S_2 ferredoxin domain from *A. aeolicus* [21], which like the *C. necator* formate dehydrogenase is known to dimerize. The largest contact interface between the two FdsBG protomers within the asymmetric unit of the crystal is between the two FdsB thioredoxin-like domains, suggesting that these contribute significantly to the dimerization of the holoenzyme.

The buried area is small (~560 $Å^2$), however, with only a few specific interactions across the interface, which are not highly conserved among the NADH dehydrogenase family. In addition, FdsBG remains monomeric throughout purification. It thus appears that the dimer seen in the asymmetric unit is simply the result of crystal packing [29,30].

8. Electron Transfer in FdsBG

During normal turnover with holoformate dehydrogenase, reducing equivalents from the oxidation of formate pass from the active site molybdenum center through a chain of iron–sulfur clusters to the FMN, which ultimately reduces NAD^+. FdsBG is able to reduce NAD^+, as are the corresponding subcomplexes from NADH dehydrogenases [31,32] and the NAD^+-reducing hydrogenase [33]. Consistent with the Fe_4S_4 cluster of FdsB being on-path between the molybdenum center and FMN, it lies close to the C8-methyl of FMN and to highly conserved surface residues that are implicated in the interaction of FdsB with FdsA (i.e., $E441^B$–$S487^B$, $I451^B$–$G452^B$, and $K292^B$–$L298^B$). By contrast, the Fe_2S_2 cluster of FdsG lies further from the region implicated in FdsA binding. Nevertheless, as summarized in Scheme 1, the present evidence indicates that the initial electron transfer event out of the FMN in FdsB upon reduction by NADH is to the off-path Fe_2S_2 cluster, which has the higher reduction potential relative to the on-path Fe_4S_4 cluster. In the case of the NADH dehydrogenases, a similar electron transfer to the Fe_2S_2 cluster is thought to minimize formation of neutral flavin semiquinone, FMNH·, thereby reducing the accumulation of reactive oxygen species [20,22].

9. Concluding Remarks

The cytosolic and NAD^+-dependent formate dehydrogenase is fully capable of catalyzing the reduction of CO_2 to formate using NADH as a source of reducing equivalents. The values for the forward and reverse steady-state kinetic parameters are consistent with the expected Haldane relationship. The addition of an NADH-regenerating system consisting of glucose and glucose dehydrogenase increases the yield of formate approximately 10-fold, suggesting the commercial potential of the enzyme as an effective means of CO_2 remediation.

A consideration of the recently reported structure of the FdhD sulfurase that transfers a catalytically essential sulfur to the maturing molybdenum cofactor prior to insertion into apoenzyme suggests that the cofactor may first be transferred to the C-terminal cap domain of apo formate dehydrogenase, which then closes over the body of the enzyme to assemble the active site, rather than transferring the cofactor directly to the body of the protein.

The X-ray crystal structure of the FdsBG fragment of the *C. necator* formate dehydrogenase is reviewed, as are the kinetics of its reduction by NADH. Notably, the neutral semiquinone FMNH· is observed transiently in the course of the reaction of FdsBG with NADH. In a reaction analogous to the physiological reduction of NADH dehydrogenases by NADH, after initial reduction of the FMN of FdsB by NADH to the hydroquinone (with a k_{red} of 680 s^{-1} and K_d of 190 μM), one electron is rapidly transferred to the Fe_2S_2 cluster of FdsG, leaving FMNH·, as characterized by both UV/visible spectroscopy and EPR. The Fe_4S_4 cluster of FdsB does not become reduced in the process.

Finally, we note that the cryo-EM structure of the *R. capsulatus* formate dehydrogenase, which is very similar to the *C. necator* enzyme that has been the focus here, has very recently been reported at a resolution of 3.3 Å [34]. The overall structure of the FdsBG fragment of the *R. capsulatus* protein is very much in agreement with that described here for the *C. necator* protein, and the overall structure is also in good agreement with that predicted previously on the basis of the structures of the *E. coli* FdhF formate dehydrogenase and the *T. thermophilus* NADH dehydrogenase [10]. Not previously anticipated is the proximity (9.5 Å edge-to-edge) of the Fe_4S_4 clusters designated A4 in the two FdsA subunits of the dimeric $Fds(ABGD)_2$ dimer, which suggests reducing equivalents are able to pass easily between protomers (a situation also seen in the even more complex formylmethanofuran dehydrogenase from *Methanothermobacter wolfeii* [35]). Interestingly, the A4 Fe_4S_4 cluster is the one possessing histidine as a ligand and presumably having a higher rather than lower reduction potential.

Importantly, the cryo-EM work clearly demonstrates that the small FdsD subunit is an integral component of the mature holoenzyme, interacting intimately with the C-terminal domain of FdsA and apparently stabilizing the inserted molybdenum cofactor. The position of FdsD is not inconsistent with the model for cofactor incorporation considered here, although its role in cofactor insertion remains to be elucidated. Very interestingly, evidence is presented that cryo-EM is able to distinguish between oxidized and reduced iron–sulfur clusters in complex systems. If found to be generally applicable, this would constitute a very significant advantage of the cryo-EM method over other structural methods and provide information presently obtainable by spatially resolved anomalous dispersion refinement [36].

Author Contributions: R.H. supervised the EPR and kinetic work described here, and prepared the manuscript. T.Y., S.H., and T.K.T. analyzed the X-ray crystallographic work with FdsBG under the supervision of G.M.B., who also contributed to preparation of the manuscript. D.N. performed the EPR and kinetic work described. X.Y. performed the work involving CO_2 reduction to formate under the supervision of A.M., who also contributed to preparation of the manuscript. All authors have read and agreed to the published version of the manuscript.

Conflicts of Interest: The authors declare no conflict of interest.

References

1. Pohlmann, A.; Fricke, W.F.; Reinecke, F.; Kusian, B.; Liesegang, H.; Cramm, R.; Eitinger, T.; Ewering, C.; Potter, M.; Schwartz, E.; et al. Genome sequence of the bioplastic-producing "Knallgas" bacterium *Ralstonia eutropha* H16. *Nat. Biotechnol.* **2006**, *24*, 1257–1262. [CrossRef] [PubMed]

2. Little, G.T.; Ehsaan, M.; Arenas-Lopez, C.; Jawed, K.; Winzer, K.; Kovacs, K.; Minton, N.P. Complete genome sequence of *Cupriavidus necator* H16 (DSM 428). *Microbiol. Resour. Announc.* **2019**, *8*. [CrossRef] [PubMed]

3. Cramm, R. Genomic view of energy metabolism in *Ralstonia eutropha* H16. *J. Mol. Microbiol. Biotechnol.* **2009**, *16*, 38–52. [CrossRef]

4. Friedebold, J.; Bowien, B. Physiological and biochemical characterization of the soluble formate dehydrogenase, a molybdoenzyme from *Alcaligenes eutrophus*. *J. Bacteriol.* **1993**, *175*, 4719–4728. [CrossRef] [PubMed]

5. Friedebold, J.; Mayer, F.; Bill, E.; Trautwein, A.X.; Bowien, B. Structural and immunological studies on the soluble formate dehydrogenase from *Alcaligenes eutrophus*. *Biol. Chem. Hoppe Seyler* **1995**, *376*, 561–568. [CrossRef] [PubMed]

6. Oh, J.I.; Bowien, B. Structural analysis of the Fds operon encoding the NAD^+-linked formate dehydrogenase of *Ralstonia eutropha*. *J. Biol. Chem.* **1998**, *273*, 26349–26360. [CrossRef] [PubMed]

7. Sazanov, L.A.; Hinchliffe, P. Structure of the hydrophilic domain of respiratory complex I from *Thermus thermophilus*. *Science* **2006**, *311*, 1430–1436. [CrossRef]

8. Berrisford, J.M.; Sazanov, L.A. Structural basis for the mecahnism of respiratory complex I. *J. Biol. Chem.* **2009**, *284*, 29773–29783. [CrossRef]

9. Efremov, R.G.; Baradaran, R.; Sazanov, L.A. The architecture of respiratory complex I. *Nature* **2010**, *465*, 441–445. [CrossRef]

10. Hille, R.; Hall, J.; Basu, P. The mononuclear molybdenum enzymes. *Chem. Rev.* **2014**, *114*, 3963–4038. [CrossRef]

11. Boyington, J.C.; Gladyshev, V.N.; Khangulov, S.V.; Stadtman, T.C.; Sun, P.D. Crystal structure of formate dehydrogenase H: Catalysis involving Mo, molybdopterin, selenocysteine, and an Fe_4S_4 cluster. *Science* **1997**, *275*, 1305–1308. [CrossRef] [PubMed]

12. Yu, X.; Niks, D.; Mulchandani, A.; Hille, R. Efficient reduction of CO_2 by the molybdenum-containing formate dehydrogenase from *Cupriavidus necator* (*Ralstonia eutropha*). *J. Biol. Chem.* **2017**, *292*, 16872–16879. [CrossRef] [PubMed]

13. Niks, D.; Duvvuru, J.; Escalona, M.; Hille, R. Spectroscopic and kinetic properties of the molybdenum-containing, NAD^+-dependent Formate Dehydrogenase from *Ralstonia eutropha*. *J. Biol. Chem.* **2016**, *291*, 1162–1174. [CrossRef] [PubMed]

14. Yu, X.; Niks, D.; Ge, X.; Liu, H.; Hille, R.; Mulchandani, A. Synthesis of formate from CO_2 gas catalyzed by an O_2-tolerant NAD^+-dependent formate dehydrogenase and glucose dehydrogenase. *Biochemistry* **2019**, *58*, 1861–1868. [CrossRef] [PubMed]

15. Thomé, R.; Gust, A.; Toci, R.; Mendel, R.; Bittner, F.; Magalon, A.; Walburger, A. A sulfurtransferase is essential for activity of formate dehydrogenase in *Escherichia coli*. *J. Biol. Chem.* **2012**, *287*, 4671–4678. [CrossRef]

16. Arnoux, P.; Ruppelt, C.; Oudouhou, F.; Lavergne, J.; Siponen, M.I.; Toci, R.; Mendel, R.R.; Bittner, F.; Pignol, D.; Magalon, A.; et al. Sulphur shuttling across a chaperone during molybdenum cofactor maturation. *Nat. Commun.* **2015**, *6*, 6148. [CrossRef]

17. Dow, J.M.; Grabel, F.; Sargent, F.; Palmer, T. Characterization of a pre-export enzyme-chaperone complex on the twin-arginine transport pathway. *Biochem. J.* **2013**, *452*, 57–66. [CrossRef]

18. Dow, J.M.; Grahl, S.; Ward, R.; Evans, R.; Byron, O.; Norman, D.G.; Palmer, T.; Sargent, F. Characterization of a periplasmic nitrate reductase in complex with its biosynthetic chaperone. *FEBS J.* **2014**, *281*, 246–260. [CrossRef]

19. Young, T.; Niks, D.; Hakopian, S.; Tam, T.K.; Yu, X.; Hille, R.; Blaha, G.M. Crystallographic and kinetic analyses of the FdsBG subcomplex of the cytosolic formate dehydrogenase from *Cupriavidus necator*. *J. Biol. Chem.* **2020**, *295*, 6570–6585. [CrossRef]

20. Schulte, M.; Frick, K.; Gnandt, E.; Jurkovic, S.; Burschel, S.; Labatzke, R.; Aierstock, K.; Fiegen, D.; Wohlwend, D.; Gerhardt, S.; et al. A mechanism to prevent production of reactive oxygen species by *Escherichia coli* respiratory complex I. *Nat. Commun.* **2019**, *10*, 2551. [CrossRef]

21. Marchler-Bauer, A.; Bo, Y.; Han, L.; He, J.; Lanczycki, C.J.; Lu, S.; Chitsaz, F.; Derbyshire, M.K.; Geer, R.C.; Gonzales, N.R.; et al. CDD/SPARCLE: Functional classification of proteins via subfamily domain architectures. *Nucleic Acids Res.* **2017**, *45*, D200–D203. [CrossRef]

22. Hinchliffe, P.; Sazanov, L.A. Organization of iron-sulfur clusters in respiratory complex I. *Science* **2005**, *309*, 771–774. [CrossRef] [PubMed]

23. Shomura, Y.; Taketa, M.; Nakashima, H.; Tai, H.; Nakagawa, H.; Ikeda, Y.; Ishii, M.; Igarashi, Y.; Nishihara, H.; Yoon, K.S.; et al. Structural basis of the redox switches in the NAD(+)-reducing soluble [NiFe]-hydrogenase. *Science* **2017**, *357*, 928–932. [CrossRef]

24. Ohnishi, T.; Ohnishi, S.T.; Salerno, J.C. Five decades of research on mitochondrial NADH-quinone oxidoreductase (complex I). *Biol. Chem.* **2018**, *399*, 1249–1264. [CrossRef] [PubMed]

25. Reda, T.; Barker, C.D.; Hirst, J. Reduction of the iron-sulfur clusters in mitochondrial NADH:ubiquinone oxidoreductase (complex I) by Eu^{II}-DTPA, a very low potential reductant. *Biochemistry* **2008**, *47*, 8885–8893. [CrossRef]

26. Edmondson, D.E.; Tollin, G. Semiquinone formation in flavo- and metalloflavoproteins. *Top. Curr. Chem.* **1983**, *108*, 109–138. [PubMed]

27. Edmondson, D.E.; Ackrell, B.A.; Kearney, E.B. Identification of neutral and anionic 8 alpha-substituted flavin semiquinones in flavoproteins by electron spin resonance spectroscopy. *Arch. Biochem. Biophys.* **1981**, *208*, 69–74. [CrossRef]

28. Palmer, G.; Mueller, F.; Massey, V. Electron Paramagnetic Resonance Studies on Flavoprotein Radicals. In *Third International Symposium of Flavins and Flavoproteins*; Kamin, H., Ed.; University Park Press: Baltimore, MD, USA, 1971; pp. 123–140.

29. Bliven, S.; Lafita, A.; Parker, A.; Capitani, G.; Duarte, J.M. Automated evaluation of quaternary structures from protein crystals. *PLoS Comput. Biol.* **2018**, *14*, e1006104. [CrossRef]

30. Krissinel, E.; Henrick, K. Inference of macromolecular assemblies from crystalline state. *J. Mol. Biol.* **2007**, *372*, 774–797. [CrossRef]

31. Yano, T.; Sled, V.D.; Ohnishi, T.; Yagi, T. Expression and characterization of the flavoprotein subcomplex composed of 50-kDa (NQO1) and 25-kDa (NQO2) subunits of the proton-translocating NADH-quinone oxidoreductase of *Paracoccus denitrificans*. *J. Biol. Chem.* **1996**, *271*, 5907–5913. [CrossRef]

32. Galante, Y.M.; Hatefi, Y. Purification and molecular and enzymic properties of mitochondrial NADH dehydrogenase. *Arch. Biochem. Biophys.* **1979**, *192*, 559–568. [CrossRef]

33. Lauterbach, L.; Idris, Z.; Vincent, K.A.; Lenz, O. Catalytic properties of the isolated diaphorase fragment of the NAD-reducing [NiFe]-hydrogenase from *Ralstonia eutropha*. *PLoS ONE* **2011**, *6*, e25939. [CrossRef] [PubMed]

34. Radon, C.; MIttelStádt, G.; Duffus, B.R.; Bürger, J. Hartmann, T.; Mielke, T.; Teutloff, C.; Leimkühler, S.; Wendler, P. Cryo-EM structures reveal intricate Fe-S cluster arrangement and charging in *Rhodobacter capsulatus* formate dehydrogenase. *Nat. Commun.* **2020**, *11*, 1912. [CrossRef] [PubMed]

35. Wagner, T.; Ermler, U.; Shima, S. The methanogenic CO2 redcuing-and-fixing enzyme is bifunctional and contains 46 [4Fe-4S] clusters. *Science* **2016**, *354*, 114–117. [CrossRef]

36. Spatzao, T.; Schlesier, J.; Burger, E.-M.; Sippel, D.; Zhang, L.; Andrade, S.L.A.; Rees, D.C.; Einsle, O. Nitrogenase FeMoCo investigated by spatially resolved anomalous dispersion refinement. *Nat. Commun.* **2016**, *7*, 10902. [CrossRef]